Damage Detection, Localization and Size Estimation Using Broadband Correlation-Based Imaging

Pierre Claude Ostiguy, Nicolas Quaegebeur, Patrice Masson

Damage detection, localization and size estimation using broadband correlation-based imaging

Pierre-Claude Ostiguy, Nicolas Quaegebeur, Patrice Masson

GAUS, Dept. of Mechanical Engineering, Université de Sherbrooke, Qc, Canada, J1K 2R1

Pierre-Claude.Ostiguy@USherbrooke.ca

ABSTRACT

Imaging approaches based on guided waves aim at detecting, locating and estimating the damage severity on a structure. The actual limitations of imaging approaches are that (1) sensitivity do damage depends on frequency used, and (2) the damage growth can be observed but not yet quantified. This paper presents a robust methodology for damage imaging and size estimation using reconstructed broadband signals, where measurements of the transfer function between each emitter and receiver are made using a sub-band decomposition strategy. Pristine transfer function is subtracted from damage transfer function signature. Imaging is conducted using a correlation-based approach (Excitelet), and dispersion compensation with reconstructed broadband signals. The approach is validated experimentally on a 1.54 mm thick aluminium plate, where only three piezoceramic transducers are bonded on the structure. Measurements are taken for two artificial damage of 13 mm and accurate detection and dimensioning is achieved. The analysis of the transfer functions using the A_0 mode shows that the wavelengths reflecting most of the energy are associated to the damage size within an accuracy of one millimetre.

KEYWORDS : *Damage imaging, guided waves, defect signature, structural health monitoring, size estimation.*

1. INTRODUCTION

Structural Health Monitoring (SHM) based on the interaction of Guided Waves (GW) with a defect are a cost-effective method for quick and continuous inspection metallic [1], composites [2] and assemblies [3]. GW approaches relies on interrogating a structure using permanently mounted transducers [4, 5]. Among these approaches, imaging algorithms aims to detect, locate and estimate the damage severity of a structure. Bonded piezoceramic (PZT) transducers are typically used as actuators and sensors to generate and measure bursts. Imaging algorithms are implemented in pitch-and-catch [1] or reflection mode (using delay-and-sum [6], Excitelet [7], dispersion compensation [8], or triangulation [9]).

Most GW damage detection algorithms are based on the estimation of Time of Flight (ToF), which requires knowledge of group velocity at a given frequency. Many approaches have proposed to process signals measured from the transducers for sparse and compact arrays [7]. Most of these algorithms use an approach similar to delay-and-sum (phased-array) with a round-robin procedure to image defects within the far field of the array. Whether these consider non-dispersive propagation, such as EUSR [10], or dispersive propagation, such as Excitelet [7], they rely on the accurate knowledge of the dispersion curves in a given frequency range [11,12], and also on the completeness of their analytical formulation [7]. Strategies for compensating the effects of dispersion have been proposed [8] to recover the shape of the input signal, and thus providing a better estimate of the ToF when coupled to delay-and-sum strategies. Model-based algorithms such as Excitelet rely on the accurate modeling of the generation, propagation and sensing of the dispersed ultrasonic GWs in the structure. For this purpose, the classical pin-force model [13] coupled to the shear lag effect [14] is usually used for the PZT, where only some aspects of the

finite geometry of the receiver are considered [15], limiting the validity range of the model to low frequencies [16]. Recent improvements in an Hybrid Pin-Force formulation allowed to improve the correlation level and to better consider the transducers dynamics up to 0.75 MHz*mm [11]. These results allow the use of broadband signals in model-based imaging. However, the generation of broadband signals involves lower energy transferred to the structure: this approach is thus affected by lower signal to noise ratio (SNR).

Most of the imaging methods uses burst excitations. However, this procedure is counter-intuitive since optimal interaction of the guided waves with defect should occur when the wavelength is of the same order than the size of the defect [17], thus defect size needs to be known to select the frequency range to be used. One method to remove this limitation would be to exploit broadband signals. Methods are presented in the literature for defect size estimation [18]. One of them consists of detecting the defect using SHM and then using an NDT method for local estimation of defect size. [18]. Other work also demonstrated that [19] defect size has an effect on guided waves. Since optimal defect interaction should be achieved when size of the defect is in the order of the wavelength, a method to estimate defect size would be to measure the transfer function of the structure and then determine which frequencies (associated to a certain wavelength) interact the most with the defect. To overcome the limitations of broadband excitation associated to low SNR, a robust methodology has been proposed in the literature to reconstruct the experimental transfer function of a structure from a sub-band decomposition technique up to 1.5 MHz [19].

In this paper, a robust methodology is proposed to detect, locate and estimate defect size, based on imaging and sub-band decomposition method to reconstruct transfer function of (i) the pristine structure and (ii) the damaged structure in order to subtract defect signature. Time domain signals are reconstructed for imaging, and then the damage signature is used to estimate defect size. Section 1 compares the standard Excitelet technique using bursts and reconstructed signals to detect and localize one defect, section 2 extends the work to multiple defects detection close to each other using reconstructed broadband signals and section 3 presents the interest of extracting the defect signature for size estimation.

2. CORRELATION-BASED IMAGING USING THE PIN-FORCE MODEL (EXCITELET)

Among the existing imaging techniques, the correlation-based Excitelet algorithm aims at reconstructing a damage index mapping of a structure by discretizing its surface into a 2D grid of equally spaced observation points (Figure 1a). For each point, a theoretical dispersed signal (traveling from the emitter to one of the receiver) is calculated assuming that there is a perfect reflection at the evaluated point. This theoretical dispersed signal is then correlated with the measurement to determine if there is damage at this point [1]. The measured signal can be reconstructed from a sub-band reconstruction as presented in [8]. The reconstruction method consists in injecting different bursts of finite frequency bandwidth in the structure and then reconstruct the transfer function of the plate [20]. This method allows reconstructing any type of excitation and increasing the SNR. Figure 1 b) presents a reconstructed transfer function of the plate prior and after a reflector is introduced, and the extracted defect signature. In this work, GWs are generated and measured using circular PZT transducers. The burst *e(t)* generated at a PZT emitter *E* propagates into the structure, and the algorithm evaluates the possible reflection at a given pixel (X_i, Y_i) coming back to the PZT receiver *R*, as shown in Fig. 1 a). For each point, the total propagation distance between the emitter *E*, the receiver *R* and the target is $d_s = d_e + d_r$. In the case of multiple transducers, the elements are actuated following standard round-robin procedure and the measurement is conducted using the other transducers.

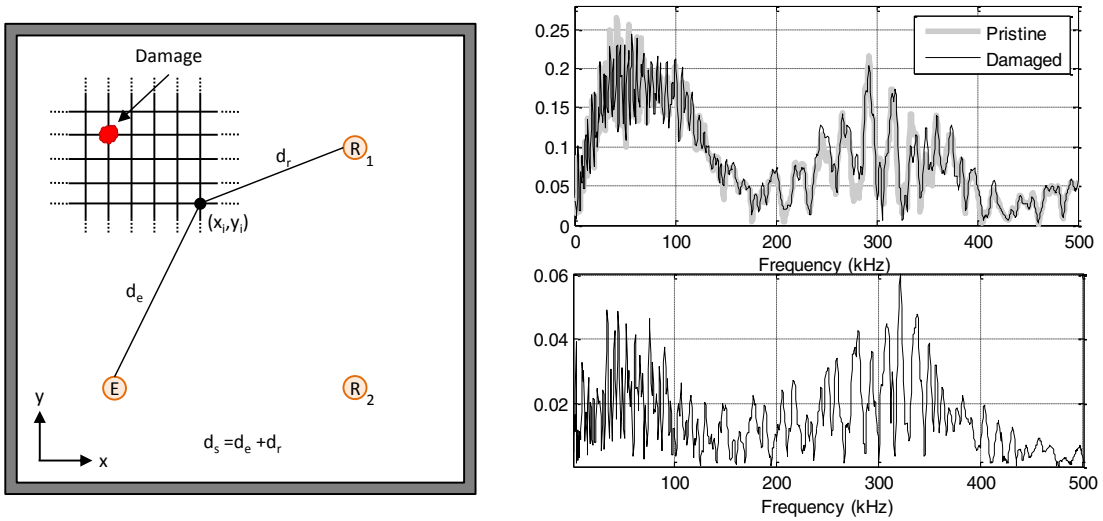

a) Imaging configuration

b) Signature of a pristine and damaged structure (top) and extracted damage signature (bottom) for one emitter-receiver pair

Figure 1. Imaging configuration for imaging, emitter (E), receiver (R) and pixel location (x_i, y_i), and damage signature in the frequency domain obtained experimentally

For each configuration of transducers and each pixel (X_i, Y_i) on the grid, the normalized correlation coefficient $c(X_i, Y_i)$ between the Hilbert transform of the theoretical signal $S_{(X_i,Y_i)}(t)$ and measured voltage signal *u(t)* is calculated over a time window *T* using the following relation:

$$c(X_i, Y_i) = \frac{\int_0^T u(t) S_{(X_i,Y_i)}(t) dt}{\sqrt{\int_0^T [u(t)]^2 dt \int_0^T \left[S_{(X_i,Y_i)}(t)\right]^2 dt}} \tag{1}$$

The use of the Hilbert transform allows smoothing the imaging results in order to provide a slightly more extended region where the correlation level is high. The GW generation and propagation model used in the present section is based on the Hybrid Pin-Force model [11], and uses a burst excitation signal $e(t)$ transformed into mechanical wave using an emitter. The main assumptions of this model are that the PZT dynamics is neglected, and the stress is integrated over the surface of the PZT receiver. Assuming isotropic propagation of a given mode, the voltage measured at the receiving PZT is thus described by the function $S_{(X_i,Y_i)}(t)$:

$$S_{(X_i,Y_i)}(t) = e(t) * P(t) \tag{2}$$

where the theoretical propagation function *P(t)* is given by [14]:

$$P(t) = \text{IFFT}\left[\sum_{\xi}\left(\tau(\omega) J_1(\xi a) \int_{d_s-c}^{d_s+c} \frac{N_s}{D_s'} \xi r H_0^{(2)}(\xi r) \tan^{-1}\left(\sqrt{\frac{4r^2 d_s^2}{(r^2 + d_s^2 - c^2)^2} - 1}\right)\right) dr\right] \tag{3}$$

where ω is the angular frequency, $\xi(\omega)$ is the wavenumber of the propagating mode (A or S), a the radius of the actuator, c the radius of the receiver, r the center-to-center distance between the transducers, J_1 is the Bessel function of first order, $H_0^{(2)}$ is the Hankel function of order 0 of the second kind, and N_s and D_s are terms that depend on the emitter dimensions [15]. While this approach takes into account the diameter of the PZT in the calculation of the propagation function, further optimization of the model is achieved by incorporating the shear-lag parameter to the model [14]. The optimized model has some limitations however, such as the experimental knowledge of

the mechanical and geometrical properties of the adhesives for which experimental evaluation is difficult.

3. EXPERIMENTAL ASSESSMENT

3.1 Experimental setup

The imaging approach is implemented for a 1.54 mm thick recrystallized 6061-T6 aluminum plate, where magnets are used as reflectors. The structure is instrumented with three circular PZTs of 10 mm diameter and 0.25 mm thickness, bonded using cyanoacrylate adhesive, and located as shown in Fig. 2. The plate is surrounded by damping tape, to reduce unwanted reflections from the boundaries. A National Instruments NI-5105 FPGA platform is used both for generation and sensing, at a sampling frequency of 6 MHz. A ProduitSon UA-8400 high voltage and large bandwidth (1 MHz) amplifier provides excitation signals up to 50 V peak. Hanning windowed bursts from 10.5 to 0.5 cycles are used with a central frequency of 200 kHz and broadband identification is conducted using sub-band decomposition for frequencies between 1kHz and 500 kHz.

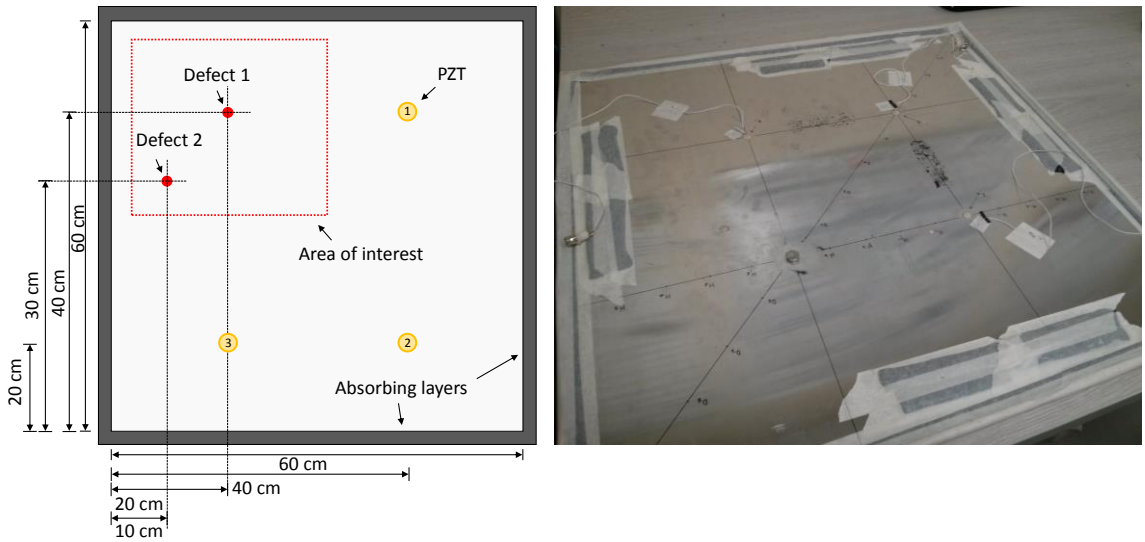

Figure 2 : Experimental setup, the dotted red line represents the section where imaging is performed

3.2 Imaging using reconstructed broadband signal

This section demonstrate the validity of using time domain signals reconstructed from broadband identification. Reconstructed signals are obtained by multiplying in the frequency domain the excitation to the signature of the reflectors, obtained by subtracting the damages signature to the pristine signature of the structure. Since the Excitelet approach has already been demonstrated to provide few false positives, only the imaging results located in the red dotted section of the plate as shown in Fig. 2 are presented. Fig. 3 presents imaging results where 2 reflectors (magnets) located at 10 cm from each other are assessed using 5.5 cycles and 0.5 cycles (Fig. 2). The imaging results obtained using the Excitelet approach and imaging based on dispersion compensation [8] technique are compared.

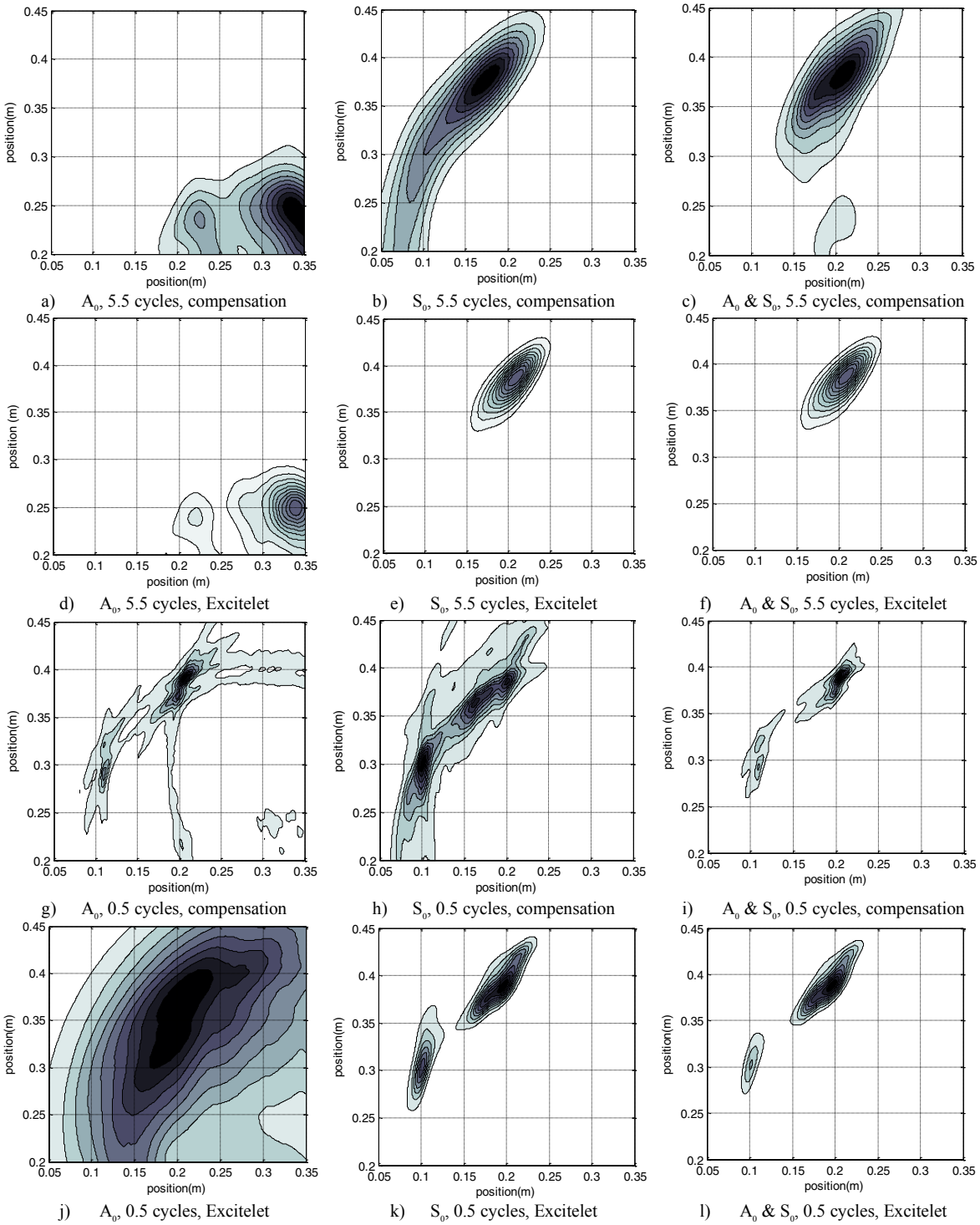

a) A_0, 5.5 cycles, compensation b) S_0, 5.5 cycles, compensation c) A_0 & S_0, 5.5 cycles, compensation

d) A_0, 5.5 cycles, Excitelet e) S_0, 5.5 cycles, Excitelet f) A_0 & S_0, 5.5 cycles, Excitelet

g) A_0, 0.5 cycles, compensation h) S_0, 0.5 cycles, compensation i) A_0 & S_0, 0.5 cycles, compensation

j) A_0, 0.5 cycles, Excitelet k) S_0, 0.5 cycles, Excitelet l) A_0 & S_0, 0.5 cycles, Excitelet

Figure 3: Comparison of imaging results of a 5.5 cycles and 0.5 cycle burst using Excitelet and the dispersion compensation technique

For both imaging methods used, it seems impossible to discriminate the 2 reflectors at 5.5 cycles either using A_0, S_0 or both modes together. However, with signals reconstructed from broadband excitation at 0.5 cycles, it is possible to discriminate defects using both modes, S_0 mode and A_0 mode in the case of the dispersion compensation technique. For both modes combined, both imaging methods give precise results. A slightly better positioning of the centre of the defect (0.1,

0.3) can be obtained with the Excitelet approach. However, the A_0 mode is too dispersive to allow an accurate positioning of both defects. Fig. 4 presents the time signals obtained after reconstruction from broadband identification, for 0.5 cycle and 5.5 cycles.

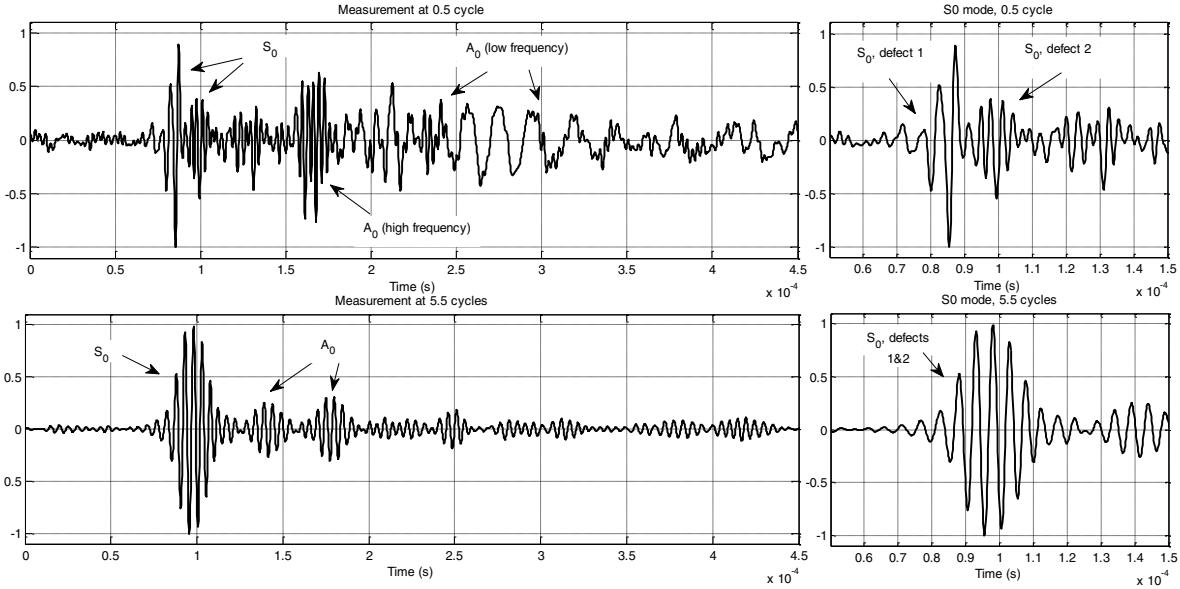

Figure 4: Comparison between a time signal obtained at 5.5 cycle and 0.5 cycles. The S_0 mode of the 0.5 cycle signal allows to separate the reflection coming from the defects, while it is not possible with a 5.5 cycles burst

At 5.5 cycles, it can be seen that the maximum correlation obtained by the A_0 mode is biased by the fact that at this frequency, the amplitude of the S_0 mode is much higher than the A_0. Since the signal is narrowband, thus the A_0 mode is also correlated with S_0 wave packets, thus leading to false results. Also, at 5.5 cycles, neither the echoes of the A_0 nor the S_0 mode coming from the two reflectors can be separated, which is not the case for a burst of 0.5 cycle. The next section details the procedure to get a first estimation of the reflector size.

3.3 Reflector size estimation based on defect signature

This section details the effect of varying reflector size on imaging results and defect signature in the frequency domain. Fig. 5 presents the imaging results obtained for reflector diameters from 6.75 mm to 18.75mm.

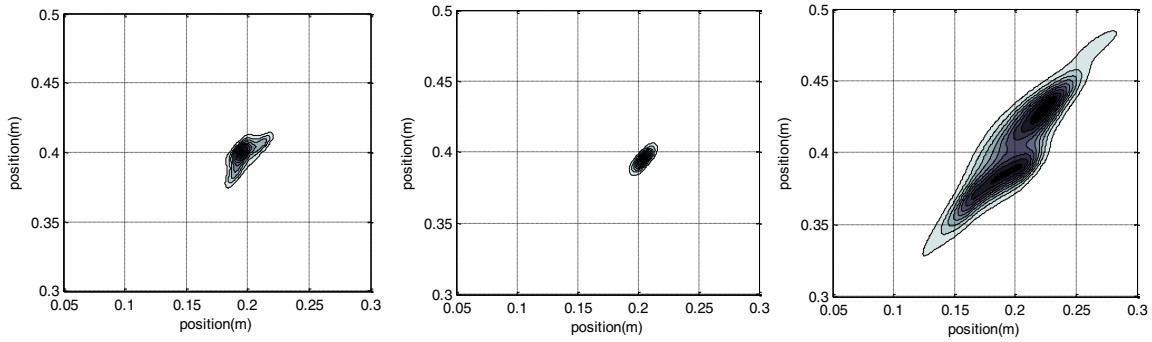

a) 6.75 mm diameter b) 13.25 mm diameter c) 18.75 mm diameter

Figure 5: Imaging results for various defect sizes

From Fig. 6, it appears that the defect size cannot be easily estimated based on the results alone. Fig. 6 shows wavelength/amplitude curves extracted from the defect signature in the frequency domain. These curves are obtained by converting the frequency axis into a wavelength axis based on the A_0 mode (more sensitive to slight variations in the reflector size due to its small wavelength).

Also, a low pass filter is applied on the measurements to smoothen the oscillations. Tab. 1 presents the characteristics of the peak with the highest reflection.

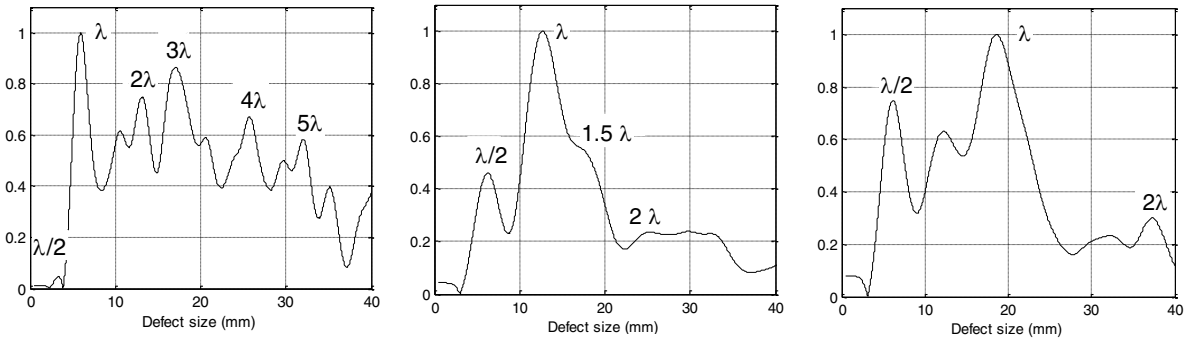

a) 6.75 mm diameter b) 13.25 mm diameter c) 18.75 mm diameter

Figure 6: Wavelength – normalized reflection amplitude graphs of the defect signature for the A_0 mode for reflectors sizes from 6.75 mm to 18 mm

Table 1: Estimated defect sizes based on the defect signature

Reflector size (mm)	Estimated size (mm)	Error (mm)	Error (%)
6.75	5.81	0.94	13.94
13.25	12.71	0.54	4.08
18.75	18.58	0.17	0.91

For all cases, the wavelength associated to the peak having the highest amplitude is close to the defect size (below 1mm). Most of the peaks with a lower amplitude can be associated to fractions of the reflector size (λ, 2 λ, λ/2, 3λ/2, 3λ). These preliminary results tend to demonstrate that using a broadband reconstruction of the transfer function of the plate prior to and after a defect is introduced, it is possible to get a first estimate of the defect size.

4. CONCLUSION

This article presents a novel strategy to exploit the broadband signature in the frequency and wavelength domains of a structure to detect, locate and provide a first estimate of the defect size within a few millimetre of accuracy. For imaging, the Excitelet approach is used and compared to the dispersion compensation approach, based on the HPF model. The signature of the defect is obtained in the frequency domain from a robust sub-band decomposition method. Imaging results show similar results as the one obtained using bursts, where the main difference between the two comes from the fact that the SNR is reduced when signals are reconstructed from the sub-band decomposition method. Multiple defects close to each other are also detected using a reduced set of three PZTs. Defect size estimation has been conducted for three defect sizes, and preliminary results show that the reflector signature allows estimating the defect size using the A_0 mode wavelengths. Further work will aim at developing a robust and autonomous methodology to estimate damage size from the defect signatures.

5. ACKNOWLEDGEMENTS

The authors would like to acknowledge the Natural and Science Research Council of Canada (NSERC) for their funding of this project.

REFERENCES

[1] P. Masson, N. Quaegebeur, and D. Langlois. A novel imaging technique for SHM using sparse and compact arrays. *Proceedings of the SPIE Health Monitoring of Structural and Biological System*, 7984, 14p., 2011.

[2] N Quaegebeur, P Micheau, P Masson, and A Maslouhi. Structural health monitoring strategy for detection of interlaminar delamination in composite plates. *Proceedings of the SPIE* Health Monitoring of Structural and Biological System, 7984, 19(8), 11p., 2011.

[3] N Quaegebeur, P Micheau, P Masson, and M Castaings. Methodology for optimal configuration in structural health monitoring of composite bonded joints. *Smart Materials and Structures*, 21(10), 2012.

[4] J.B. Ihn and F.K. Chang. Pitch-catch active sensing methods in structural health monitoring for aircraft structures. *Structural Health Monitoring*, 7, 11p., 2008.

[5] V. Giurgiutiu, A. Zagrai, and J. Bao. Piezoelectric wafer embedded active sensors for aging aircraft structural health monitoring. *Structural Health Monitoring*, 1(1), 20p., 2002.

[6] Giurgiutiu, V., Structural Health Monitoring with Piexoelectric Wafer Active sensors. *Academic Press*, 2008

[7] Quaegebeur, N., Masson, P., Langlois-Demers, D., Micheau, P. Dispersion-based imaging for structural health monitoring using sparse and compact arrays. *Smart Materials and Structures,* 20, 12p., 2011.

[8] P.D. Wilcox. A rapid signal processing technique to remove the effect of dispersion from guided wave signals. *IEEE Transactions on Ultrasonic, Ferroelectric and Frequency Control*, 50(4), 8p., 2003.

[9] G. Giridhara, V.T. Rathod, S. Naik, D. Roy Mahapatra, S. Gopalakrishnan, Rapid localization of damage using a circular sensor array and Lamb wave based triangulation, *Mechanical Systems and Signal Processing,* 24(8), 17p., 2010.

[10] V. Giurgiutiu. Tuned lamb wave excitation and detection with piezo-electric wafer active sensors for structural health monitoring. *Journal of Intelligent Material Systems and Structures*, 16(4), 2005.

[11] Ostiguy, P.-C., Quaegebeur, N. and Masson, P. Improved damage imaging in aerospace structures using a piezoceramic hybrid pin-force wave generation model, *Proceedings of the SPIE conferences,* 12p. 2014.

[12] Ostiguy, P.-C., Quaegebeur, N., Mulligan, K. R., Masson, P. and Elkoun, S. In-situ mechanical characterization of isotropic structures using guided wave propagation, *Smart Materials and Structures*, 21(6), 2012.

[13] Raghavan, A. and Cesnik, C.E.S., Finite-Dimensionsl Piezoelectric Trandsucer Modelling for Guided Wave based Structural Health Monitoring. *Smart Materials and Structures,* 14, 13p., 2005.

[14] L. Yu, G. Bottai-Santoni, and V. Giurgiutiu. Shear lag solution for tuning ultrasonic piezoelectric wafer active sensors with applications to lamb wave array imaging. *International Journal of Engineering Science*, 13p., 2010.

[15] Sohn, H. and Lee, S.J., Lamb wave tuning curve calibration for Surface-Bonded Piezoelectric Transducers. *Smart Materials and Structures*, 19, 15p., 2010.

[16] Quaegebeur, N., Ostiguy, P.-C. and Masson, P. Correlation-based imaging algorithm for fatigue monitoring of riveted lap-joint structure. *Smart Materials and Structures* 23, 15p., 2014.

[17] Alleyne, D. N. and Cawley, P. Optimization of Lamb wave inspection techniques. *NDT&E International,* 25(1), 12p., 1992.

[18] J. E. Michaels ; A. J. Dawson ; T. E. Michaels and M. Ruzzene. Approaches to hybrid SHM and NDE of composite aerospace structures, *Proceedings of the SPIE conferences 2014*, 2014.

[19] N. Hu, T. Shimomukai, H. Fukunaga, and Z. Su. Damage identification of metallic structures using A0 mode of lamb waves. *Structural Health Monitoring*, 7, 15p., 2008.

[20] Quaegebeur, N., Masson, P. Micheau, P. and Mrad, N. Broadband generation of ultrasonic guided waves using sub-band decomposition, *IEEE Transactions on Ultrasonics, Ferroelectrics and Frequency control*, 59(5), 10p., 2012.

[21] Raghavan, A. and Cesnik, C.E.S., Finite-Dimensionsl Piezoelectric Trandsucer Modelling for Guided Wave based Structural Health Monitoring, *Smart Materials and Structures* 14, 13p., 2005.